

# Performance of a large TeO<sub>2</sub> crystal as a cryogenic bolometer in searching for neutrinoless double beta decay

L. Cardani<sup>a,b</sup>, L. Gironi<sup>c,d</sup>, J.W. Beeman<sup>e</sup>, I. Dafinei<sup>a</sup>, Z. Ge<sup>f</sup>, G. Pessina<sup>c</sup>, S. Pirro<sup>c,\*</sup>, Y. Zhu<sup>f</sup>

<sup>a</sup>INFN - Sezione di Roma 1 I 00185 Roma - Italy

<sup>b</sup>Dipartimento di Fisica - Università di Roma La Sapienza I 00185 Roma - Italy

<sup>c</sup>INFN - Sezione di Milano Bicocca I 20126 Milano - Italy

<sup>d</sup>Dipartimento di Fisica - Università di Milano Bicocca I 20126 Milano - Italy

<sup>e</sup>Lawrence Berkeley National Laboratory, Berkeley, California 94720, USA

<sup>f</sup>Shanghai Institute of Ceramics, Chinese Academy of Science, Shanghai 200050, PR China

## Abstract

Bolometers are ideal devices in the search for neutrinoless Double Beta Decay (0νDBD). Enlarging the mass of individual detectors would simplify the construction of a large experiment, but would also decrease the background per unit mass induced by  $\alpha$ -emitters located close to the surfaces and background arising from external and internal  $\gamma$ 's. We present the very promising results obtained with a 2.13 kg TeO<sub>2</sub> crystal. This bolometer, cooled down to a temperature of 10.5 mK in a dilution refrigerator located deep underground in the Gran Sasso National Laboratories, represents the largest thermal detector ever operated. The detector exhibited an energy resolution spanning a range from 3.9 keV (at 145 keV) to 7.8 keV (at the 2615  $\gamma$ -line of <sup>208</sup>Tl) FWHM. We discuss the decrease in the background per unit mass that can be achieved increasing the mass of a bolometer.

**Keywords:** TeO<sub>2</sub> crystals, Bolometers, Double Beta Decay

**PACS:** 07.20.Mc, 29.30.Ev, 29.30.Kv, 29.40.Vj

## 1. Introduction

Neutrinoless Double Beta Decay (0νDBD) is a rare nuclear process hypothesized to occur in certain nuclei. If observed, it would give important information about the properties of the neutrino and the weak interaction. Double Beta Decay searches [1, 2, 3] gained critical importance after the discovery of neutrino oscillations and many experiments are concluding R&D and other are now under construction.

Thermal bolometers are ideal detectors for this survey because they can be composed by most of the more interesting  $2\beta$ -emitters and, fundamental for next generation experiments, they show an excellent energy resolution. The Cuoricino experiment [4], which constituted of an array of 62 TeO<sub>2</sub> (750 g) crystal bolometers, demonstrated the power of this technique and established the basis for the CUORE experiment [5], which will operate 988 TeO<sub>2</sub> crystals of the same size. In addition to <sup>130</sup>Te,  $2\beta$ -scintillating bolometers [6] based on <sup>116</sup>Cd [7], <sup>100</sup>Mo [8, 9], and <sup>82</sup>Se [10] were recently operated with success.

In such experiments, increasing the mass of the individual detector module can be extremely helpful, for several reasons. First, it improves the Peak-to-Compton ratio for  $\gamma$ -ray interactions, enabling not only better identification of environmental background but also decreasing the continuum induced by Compton and multi-Compton scattering. Second, the reduction in the surface-to-volume ratio reduces the background per

unit mass from surface impurities [11]. Moreover, the total  $2\beta$ -efficiency (related to the full containment of the 2 e<sup>-</sup> emitted in the decay) of the detector will slightly increase. Last, a large-mass experiment inevitably requires the use of an array of detectors, so a larger individual detector corresponds to a lower number of readout channels, and a simpler setup.

## 2. Growth of a 2.13 kg TeO<sub>2</sub> crystal

The TeO<sub>2</sub> crystal studied in this work was grown using the modified Bridgman method, described in detail in previous articles [12, 13]. The main challenge in growing very large crystals using this technique consists in maintaining an adequate thermal compensation during all stages of its growth, especially in the last (Fig. 1). Thermal compensation is needed to guarantee the flat or slightly convex liquidus-solidus (LS) interface essential to obtaining a good crystal perfection along the whole ingot. One of the peculiarities of our growth method is that the seed end of the crucible remains outside the furnace cavity (i.e. in open air) during all stages of growth, so controlling the LS interface is very difficult. Moreover, in the final stage almost the entire crucible is exposed to open air resulting in sizable thermal radiation with the need of thermal compensation. In the particular case of growing a very large crystal the thermal compensation was even more critical and required implementing different thermal compensation rates during the growth of an approximately 2.5 kg TeO<sub>2</sub> ingot. In the final phase of cutting and polishing the as-grown ingot, a compromise was adopted

\*Corresponding author

Email address: Stefano.Pirro@mib.infn.it (S. Pirro)

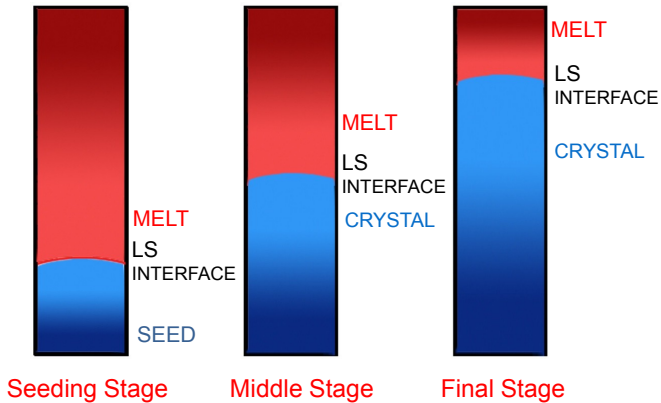


Figure 1: Sketch map of the growth stages in Bridgman method.

in order to maximize the crystal weight while maintaining a reasonable shape and quality standards. In particular, two of the crystal corners were discarded, corresponding to roughly  $2 \text{ cm}^3$ . Some inclusions are present close to one of the crystal faces. The final crystal shows a slightly truncated-pyramidal shape with a rectangular cross section. The dimensions of the boundary sections are  $54.7 \times 59.6 \text{ mm}^2$  and  $54.0 \times 58.2 \text{ mm}^2$ . The length is  $111.3 \text{ mm}$  and its total weight is  $2.133 \text{ kg}$ .

### 3. Experimental details

The  $\text{TeO}_2$  crystal bolometer is secured by means of eight S-shaped PTFE supports mounted on Cu columns (Fig. 2); this is the simplest way to hold a crystal of non-standard shape. The S-shape of the Teflon supports ensures that with the decrease of the temperature the crystal is clasped tighter, due to the fact that the thermal contraction of PTFE is larger than  $\text{TeO}_2$ . The temperature sensor is a  $3 \times 3 \times 1 \text{ mm}^3$  neutron transmutation doped Germanium thermistor, identical to the ones used in the Cuorino experiment. It is thermally coupled to the crystal via 9 glue spots of  $\sim 0.6 \text{ mm}$  diameter and  $\sim 50 \mu\text{m}$  height. In addition, a  $\sim 300 \text{ k}\Omega$  resistor made of a heavily doped meander on a  $3.5 \text{ mm}^3$  silicon chip, is attached to each crystal and acts as a heater to stabilize the gain of the bolometer [14, 15]. The  $50 \mu\text{m}$  gold wires ball-bonded on thermistor and heater are crimped into  $0.65 \text{ mm}$  copper tubes (“male” pin) inserted into larger copper tubes (“female” pin) glued (electrically insulated) on a copper plate. Twisted constantan wires having a diameter  $60 \mu\text{m}$  (not shown in Fig. 2) are crimped in similar Cu tubes on the opposite end of the female connectors and carry the electrical signal up to the cryostat’s Mixing Chamber, where a custom wiring brings the electrical signal up to the front-end electronics, located just outside the cryostat.

The detector was operated deep underground in the Gran Sasso National Laboratories in the CUORE R&D test cryostat. The details of the the cryogenic facility and its electronics can be found elsewhere [16, 17, 18, 19].

Heat pulses, produced by particle interactions in the  $\text{TeO}_2$  crystal are transduced into voltage pulses by the NTD thermistor, and are then amplified and fed into a 16 bit NI 6225 USB

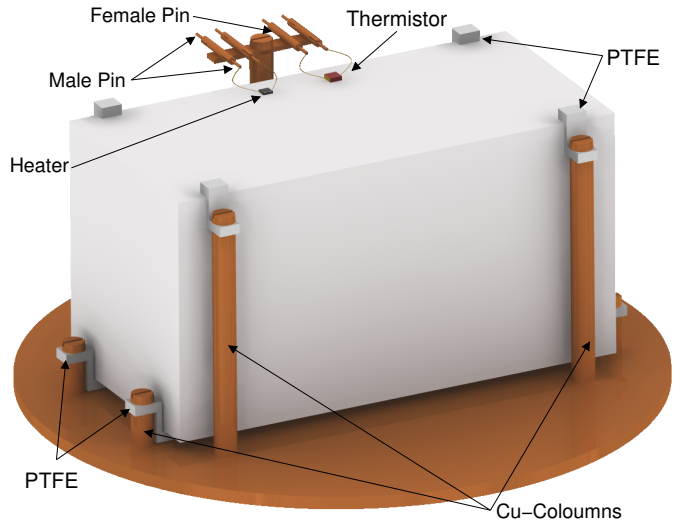


Figure 2: The detector setup. The crystal is held by means of eight S-shaped PTFE supports mounted on Cu columns. The thermistors and the heater contacts are realized through crimped Cu pipes glued on a Cu plate. The entire setup is enclosed inside a Cu shield kept at base temperature.

ADC unit. The entire waveform (“raw pulse”) of each triggered voltage pulse is sampled and acquired. The amplitude and the shape of the voltage pulse is then determined by an off line analysis which uses the Optimum Filter (O.F.) technique [5, 20]. The signal amplitude is computed as the maximum of the optimally filtered pulse, while the signal shape is evaluated on the basis of several different parameters: the rise time ( $\tau_{rise}$ ) and the decay time ( $\tau_{decay}$ ) are evaluated from the raw pulse as  $(t_{90\%} - t_{10\%})$  and  $(t_{30\%} - t_{90\%})$ , respectively.

### 4. Detector Performances

The detector was operated at a temperature of  $\approx 10.5 \text{ mK}$ . The corresponding working resistance of the thermistor was  $65 \text{ M}\Omega$ . The main characteristics of the detector are reported in Tab. 1.

Table 1: Main parameters of the crystal bolometer. The second column represents the theoretical resolution given by the Optimum Filter. The last column represents the absolute signal read out across the thermistor. The electronics has a six-pole Bessel filtering stage at  $12 \text{ Hz}$ .

R	FWHM (O.F.)	$T_{rise}$	$T_{decay}$	Signal
[ $\text{M}\Omega$ ]	[keV]	[ms]	[ms]	[ $\mu\text{V}/\text{MeV}$ ]
65	3.7	29	95	24

The most remarkable feature of this large bolometer is the signal shape. In particular, the decay time shows two unexpected features: it abruptly decreases to  $\sim 8\%$  of the signal height and then shows an extremely long decay constant. An example of this behaviour is presented in Fig. 3, along with the

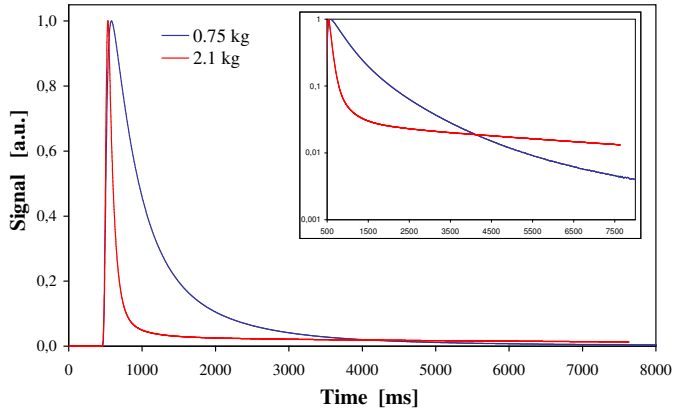


Figure 3: Average thermal pulse obtained for the 2.1 kg crystal under study (light red). For comparison we also plot the average pulse obtained with 750 g  $\text{TeO}_2$  crystal (dark blue) under similar conditions (temperature and resistance). The signals are normalized to the rising edge. The inset shows that the 2.1 kg crystal has a predominant fast decay and a second, very slow decay constant. Also the rise time of the large crystal results  $\approx 2$  times faster with respect to the smaller crystal.

average thermal pulse<sup>1</sup> of a Cuoricino (750 g)  $\text{TeO}_2$  crystal for comparison.

The mean signal decay time observed in the Cuoricino experiment was of the order of  $\sim 250$  ms, while the mean rise time was of the order of  $\sim 80$  ms. From a theoretical point of view the decay time for a perfect crystal is given by  $\tau=C/G$ , where  $C$  represents the heat capacity of the crystal ( $\propto$  mass) and  $G$  is the thermal link to the heat sink (dominated by the PTFE supports). Given the fact that the PTFE supports used in Cuoricino were identical in shape and number, one would have expected a decay time of the order of  $\approx 700$  ms instead of 95 ms. In fact this behaviour is observed in crystal absorbers in which the crystal structure exhibits some defects. In the specific case of  $\text{TeO}_2$  crystals, this behaviour was observed in the enriched ones (operated in Cuoricino) which, being the only “imperfect”  $\text{TeO}_2$  tested up to now, show a pulse shape very similar to the one observed in our large crystal under study.

The second characteristic that is normally associated with non perfect crystal lattices (often resulting also in polycrystalline structures) is a reduction in the absolute signal height. The observed value of  $24 \mu\text{V}/\text{MeV}$  is rather small when compared with the mean value of  $\sim 150 \mu\text{V}/\text{MeV}$  observed in Cuoricino at a similar working resistance (i.e. temperature) [22]. We believe that this unusual thermal response can be definitely ascribed to the imperfections present in the crystal, as described in Sec. 2. These imperfections normally imply a degradation in the energy resolution of the device as well. This can be qualitatively described in terms of position effects due to localized imperfections in which the interacting particle could thermalize slightly differently. As example, in Cuoricino the mean FWHM energy resolution of the enriched crystals (evaluated at 2615 keV) was  $\approx 15$  keV, while the resolution of the

<sup>1</sup>The average thermal pulse, i.e. the shape of a pulse in absence of noise, is computed from a proper average of a large number of raw pulses.

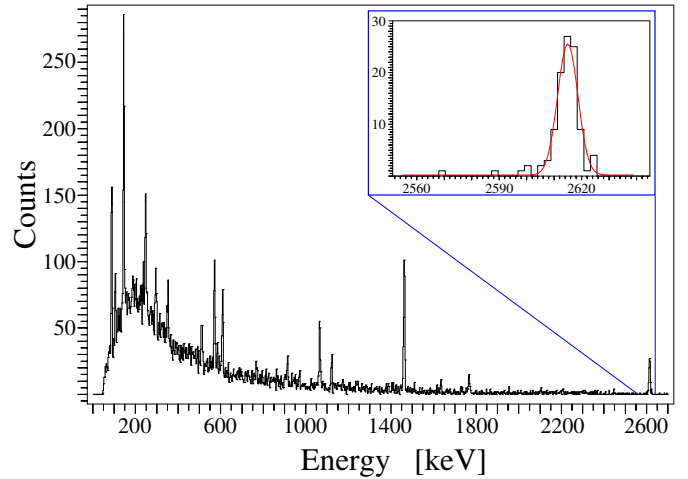


Figure 4: The 2.1 kg crystal’s calibration spectrum. The most prominent low-energy lines are due to internal contaminations of  $^{121m}\text{Te}$ ,  $^{123m}\text{Te}$ ,  $^{125m}\text{Te}$ ,  $^{127m}\text{Te}$  and  $^{129m}\text{Te}$ , activated during the shipment by airplane. Due to the high counting rate a weak  $^{232}\text{Th}$  source was used, in order to avoid pile-up. The corresponding  $^{208}\text{Tl}$  2615 keV  $\gamma$ -line is highlighted. The 1461 keV line is due to  $^{40}\text{K}$  environmental contamination.

same-sized ( $3\times 3\times 6 \text{ cm}^3$ ) natural crystal was  $\approx 9$  keV [4].

In Fig. 4 we present the calibration spectrum obtained with the 2.1 kg crystal. All the observed low-energy lines are due to internal contaminations of metastable Te isotopes activated through fast neutron interactions which occurred during shipping (15 hours via airplane, from Shanghai to Rome). The most intense low-energy lines are 88 keV ( $^{127m}\text{Te}$ ), 105 keV ( $^{129m}\text{Te}$ ), 145 keV ( $^{125m}\text{Te}$ ), 247 keV ( $^{123m}\text{Te}$ ) and 294 keV ( $^{121m}\text{Te}$ ). The line at 1064 keV is due, instead, to the presence of another sample, namely a  $5\times 5\times 5 \text{ cm}^3$  BGO crystal, located a few cm away in the same setup.  $^{207}\text{Bi}$  is a typical BGO contamination that shows a particular  $\gamma$  emission at 1064 keV. Finally, the 1461 keV line is due to environmental  $^{40}\text{K}$  contamination, while the 2615 keV line arises from the external  $^{232}\text{Th}$  source. The FWHM energy resolutions evaluated on the most intense lines are presented in Tab. 2.

Table 2: FWHM energy resolutions (in keV) evaluated from the calibration spectrum of Fig. 2. †The resolution is evaluated on the right (Gaussian) tail of the peak (see Fig. 5).

145 keV	571 keV	1461 keV	2615 keV	5407 keV
$3.9 \pm 3$	$4.7 \pm 4$	$6.6 \pm 3$	$7.8 \pm 7$	$7.8 \pm 2$ †

All the  $\text{TeO}_2$  crystals produced so far show a contamination in  $^{210}\text{Po}$ . This contamination does not represent a serious problem for DBD searches since it has a “relatively short” decay time ( $T_{1/2}=138$  days) and is an almost pure  $\alpha$ -decay. Furthermore, it seems that  $^{210}\text{Po}$  is normally homogeneously distributed in the bulk so that in fact it represents a natural calibration and stabilization line. In this case, however, we observed a rather high contamination, of the order of 0.026 Bq. The total acquisition rate of the detector during measurement was 0.13

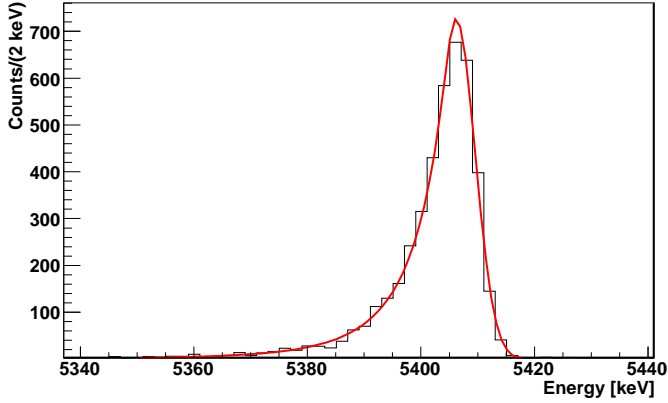


Figure 5: The  $\alpha$ +recoil peak due to internal contamination of  $^{210}\text{Po}$ . The fit, performed with the Crystal Ball function, is shown in red.

Hz. This relatively high rate (both in the  $\beta$  and  $\alpha$  regions) combined with the extremely long tail of the thermal pulses results in a sort of “permanent” pile-up. As an example, from Fig. 3 it can be evaluated that  $\sim 7$  sec after a  $^{210}\text{Po}$  decay the baseline is still at 1.3 % of its maximum value. Very naively one can calculate that at this point the bolometer still has to “dissipate” an amount of heat (i.e. energy) of roughly  $1.3\% \times 5407 \text{ keV} \approx 70 \text{ keV}$ . This value is rather high when compared with the energy resolution presented in Tab. 2.

In effect, then, iso-energy events will be randomly distributed over a decreasing tail (mostly induced by  $^{210}\text{Po}$ ) whose amplitude variation can represent a large fraction with respect to the one induced by a random event. This will affect the energy resolution.

The peak due to the  $^{210}\text{Po}$  decay is presented in Fig. 5. It can be noted that the peak presents a long non-Gaussian tail on its left side. We do not have a clear explanation for this feature, even though we think it could be partially related to the high event rate of the detector. The tail could also be induced by an anomalous  $^{210}\text{Po}$  concentration close to the surfaces of the crystal. This is rather difficult to evaluate but it cannot be excluded considering what was discussed in Sec. 2. The peak is fitted with the Crystal Ball function [23], which is commonly used to model various lossy processes in high-energy physics. The function consists of a Gaussian core portion and a power-law low-end tail, below a certain threshold. As a final remark we would like to point out that even if the absolute signal height ( $24 \mu\text{V}/\text{MeV}$ ) was a factor of 1/2 less than the expected one, the noise due to the electronic chain ( $5 \div 10 \text{ nV Hz}^{-1/2}$ ) is negligible and can be estimated (for this detector) as 1.2 keV FWHM.

## 5. Background considerations

The main sources of background for  $\text{TeO}_2$  bolometers [11] are due to:

- $\alpha$ -emitters located on or close to the surface of a detector.
- Environmental  $\gamma$ -emitters, mostly arising from  $^{232}\text{Th}$  decay chain.

Both contributions can be reduced by increasing the size of the crystal.

Surface contamination represents the a major source of background for the Cuoricino and CUORE experiments. Since this background is proportional to the active surface of the crystal, while the DBD signal is proportional to the mass, decreasing the surface-to-volume ratio will result in an increase of the signal over background ratio.

If for example we compare a  $7.1 \times 7.1 \times 7.1 \text{ cm}^3$   $\text{TeO}_2$  crystal (which corresponds to a mass of 2.13 kg) to a  $5 \times 5 \times 5 \text{ cm}^3$  CUORE crystal we find the background per unit mass will be smaller by a factor given by the ratio of their sides,  $7.1/5 = 1.42$ . Though this may not seem like a large number, it must be taken into account that the sensitivity of a DBD experiment is directly proportional to  $(\text{Detector Mass}/\text{Background})^{1/2}$ .

The second background effect originates from the environmental  $\gamma$  radioactivity. Before discussing the relationship between the size of the crystal detector and the background level due to environmental  $\gamma$  radiation, it is useful to briefly describe the main contributions to this background in the energy region 2500–2600 keV, since the DBD peak of  $^{130}\text{Te}$  is expected at 2528 keV.

The background in this region is largely dominated by the  $\beta$  decay of  $^{208}\text{Tl}$ , belonging to the  $^{232}\text{Th}$  chain. Several high-energy  $\gamma$ 's are emitted within this transition, the dominant being the 2615 keV  $\gamma$ -line, emitted with a Branching Ratio (BR) of 99%. Due to the extremely high transition energy of the decay (5001 keV), a cascade of other high-energy  $\gamma$ 's are emitted simultaneously, the main ones being at 277 keV, 583 keV and 860 keV.

In order to understand the background, we distinguish two different mechanisms, both involving the 2615 keV  $\gamma$  line:

1. multi-Compton events of the 2615 keV  $\gamma$ -line of  $^{208}\text{Tl}$ .
2. multi-Compton events of the 2615 keV  $\gamma$ -line, with the simultaneous interaction of a second  $\gamma$  in the crystal.

Both of these contributions vary according to the size of the detector. In the first case, an increase in the crystal size increases the probability that a  $\gamma$ , after several Compton interactions, releases all of its energy inside the crystal, with a consequent *improvement* of the peak-to-multi-Compton ratio.

In the second case, however, with a larger crystal there is an increased probability for two  $\gamma$ 's to interact simultaneously in the crystal thus *increasing* the background level. This contribution strongly depends on the distance between the source and the crystal.

In order to better evaluate the background per unit mass, several Monte Carlo simulations (GEANT4) have been run in which the distance between the source and crystals of different size was varied. In order to have enough statistics (especially for large distances) we defined the Region Of Interest (ROI) as the energy interval between 2500 keV and 2600 keV. We simulated point-like sources placed at various distances from a  $5 \times 5 \times 5 \text{ cm}^3$  and a  $7 \times 7 \times 7 \text{ cm}^3$   $\text{TeO}_2$  crystals. In order to better understand the contribution due to the two above mentioned mechanisms, we simulated two different sources: a *complete*  $^{232}\text{Th}$  decay chain, corresponding to a real physical case and a second

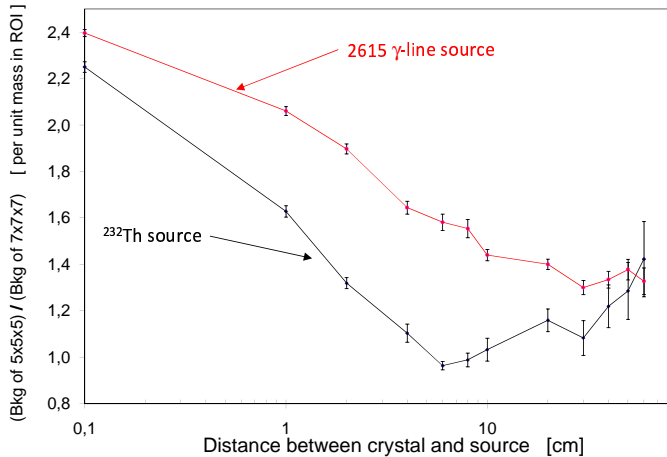


Figure 6: Ratio of the events per unit mass of a  $5 \times 5 \times 5$  cm<sup>3</sup> crystal with respect to a  $7 \times 7 \times 7$  cm<sup>3</sup> crystal evaluated in the ROI, as a function of the distance between crystal and source. The black points are obtained simulating a point-like “real” <sup>232</sup>Th source, while the red points relate to a single 2615 keV  $\gamma$ -line source. The error bars are due to statistical error and correspond to one  $\sigma$ -level. The lines through the data points are only to guide eyes.

one consisting of a single 2615 keV  $\gamma$ -line emission. In this way the contribution of the two mechanisms as a function of the distance between crystal and source can be disentangled.

In Fig. 6 we show the results of the simulations. We plot the ratio between the number of counts (within the ROI) per unit mass obtained with a  $5 \times 5 \times 5$  cm<sup>3</sup> crystal with respect to the same for a  $7 \times 7 \times 7$  cm<sup>3</sup> crystal, as a function of the distance between the source and the crystals.

As it can be seen, the background in the ROI for sources very close or very far from the crystal is significantly lower for larger crystals. For intermediate distances, where coincidences dominate, this difference is less significant. This can be explained in a simple way. When the point-like source is very close to the crystal surface, the coincidence probability does not depend strongly on crystal dimensions since it covers almost half of the solid angle. Once the distance of the source from the detector increases and becomes of the same size of the crystal dimensions then the *difference* in the coincidence probability of the two crystals reaches its maximum, just due to a solid angle effect. When the distance from the crystal further increases, the difference in the coincidence probability decreases again and becomes negligible. We also performed simulations considering a diffused <sup>232</sup>Th source within a “support material” (such as Cu, widely used for thermal detectors) and varying the distance of this support from the crystal. Apart from the time needed for the simulation to accumulate enough events in the ROI, the ratio of the background per unit mass is very close to the one reported in Fig. 6.

We also performed some simulations considering <sup>214</sup>Bi, the most troublesome radionuclide of the <sup>238</sup>U chain. In this case we obtained only very small differences between crystals of different size. This is probably due to the fact that in <sup>214</sup>Bi  $\beta$ -decay there is an enormous number of  $\gamma$ 's emitted simultaneously. In this case, the term due to coincidences dominates with respect

to the Multi-Compton term, resulting in a very small difference in the background per unit mass. For the sake of completeness it should be remarked that for experiments based on DBD emitters whose transition energy does not exceed 2615 keV, the main source of environmental radioactivity is dominated by <sup>232</sup>Th trace contaminations. This is simply due to the fact that the BR of <sup>214</sup>Bi into high energy  $\gamma$ 's is  $\sim 0.15$  % for the <sup>238</sup>U decay chain, while in the case of <sup>208</sup>Tl the BR into the 2615 keV line is 36 % for the <sup>232</sup>Th decay chain.

We conclude by pointing out that the efficiency of containing the  $2 e^-$  of the  $0\nu\text{DBD}$  will increase from 87.4 % for a 0.75 kg crystal to 91.5 % for a 2.13 kg crystal.

## 6. Conclusions

We successfully tested a 2.1 kg TeO<sub>2</sub> crystal as a thermal bolometer, the largest such detector to date. Despite the presence of imperfections in the crystal, the detector energy resolution in the  $0\nu\text{DBD}$  region is the same as that obtained in the Cuoricino experiment. The advantages of using larger mass crystals for  $0\nu\text{DBD}$  decay searches was simulated and discussed. We strongly believe that our technique is capable of operating multi-kg crystal detectors (composed by different  $\beta\beta$ -emitters) with the required energy resolution in the  $2 \div 3$  MeV energy window. There is room for improvement in crystal quality and thus in pulse shape and energy resolution as well. The current sample came from a routine production, so better-quality large crystals could be obtained if dedicated furnaces were used.

## 7. Acknowledgements

Thanks are due to the LNGS mechanical workshop, in particular to E. Tatananni, A. Rotilio, A. Corsi, B. Romualdi and F. De Amicis for their continuous and constructive help in each aspect of detector design and construction. We are especially grateful to Maurizio Perego for his invaluable help in the development and improvement of the data acquisition software.

## 8. References

### References

- [1] F.T. Avignone III, S.R. Elliott, J. Engel, Rev. Mod. Phys. 80 (2008) 481.
- [2] G. L. Fogli et al., Phys. Rev. D 78 (2008) 033010.
- [3] A. Strumia and F. Vissani, [hep-ph/0606054v3] (2010).
- [4] E. Andreotti et al., Astropart. Phys. 34 (2011) 822.
- [5] C. Arnaboldi et al., Nucl. Instr. and Meth. A 518 (2004) 775.
- [6] S. Pirro et al., Physics of Atomic Nuclei 69 (2006) 2109. [nucl-ex/0510074].
- [7] C. Arnaboldi et al., Astropart. Phys. 34 (2010) 143.
- [8] L. Gironi et al., 2010 JINST 5 P11007.
- [9] L. Gironi, Nucl. Instr. and Meth. A 617 (2010) 478.
- [10] C. Arnaboldi et al., Astropart. Phys. 34 (2011) 344.
- [11] M. Pavan et al., Eur. Phys. J A 36 (2008) 159.
- [12] Y. Chu et al., Journal of Crystal Growth 295 (2006) 158.
- [13] C. Arnaboldi et al., Journal of Crystal Growth 312 (2010) 2999.
- [14] A. Alessandrello et al., Nucl. Instr. and Meth. A 412 (1998) 454.
- [15] C. Arnaboldi, G. Pessina, E. Previtali, IEEE Trans. on Nucl. Sci. 50 (2003) 979.

- [16] C. Arnaboldi et al., IEEE Trans. on Nucl. Sci. 49 (2002) 2440.
- [17] C. Arnaboldi et al., Nucl. Instr. and Meth. A 520 (2004) 578.
- [18] S. Pirro, Nucl. Instr. and Meth. A 559 (2006) 672.
- [19] C. Arnaboldi, G. Pessina, S. Pirro, Nucl. Instr. and Meth. A 559 (2006) 826.
- [20] E. Gatti and P.F. Manfredi, Rivista del Nuovo Cimento 9 (1986) 1.
- [21] C. Arnaboldi et al., Phys. Rev. C 78 (2008) 035502.
- [22] S. Pirro et al., Nucl. Instr. and Meth. A 559 (2006) 352.
- [23] E. Gaiser, Ph.D. Thesis, SLAC-R-255 (1982) 178;  
<http://root.cern.ch/root/html/RooCBSShape.html>